Enhancement of the Superconducting Gap by Nesting in CaKFe_{4}As_{4}: A New High Temperature Superconductor

Daixiang Mou, Tai Kong, William R. Meier, Felix Lochner, Lin-Lin Wang, Qisheng Lin, Yun Wu, S. L. Bud'ko, Ilya Eremin, D. D. Johnson, P. C. Canfield, and Adam Kaminski

Phys. Rev. Lett. **117**, 277001 — Published 28 December 2016

DOI: 10.1103/PhysRevLett.117.277001

Deviation from $s^{\pm}$ pairing symmetry in new high-temperature superconductor $CaKFe_4As_4$

Daixiang Mou[1,2], Tai Kong[1,2], William R. Meier[1,2], Felix Lochner[3], Lin-Lin Wang[2], Qisheng Lin[1], Yun Wu[1,2], S. L. Bud'ko[1,2], Ilya Eremin[3], D. D. Johnson[1,2,4], P. C. Canfield[1,2], Adam Kaminski[1,2]

[1] *Division of Materials Science and Engineering, Ames Laboratory, Ames, Iowa 50011, USA*

[2] *Department of Physics and Astronomy, Iowa State University, Ames, Iowa 50011, USA*

[3] *Institut fur Theoretische Physik III, Ruhr-Universitat Bochum, 44801 Bochum, Germany*

[4] *Department of Materials Science and Engineering, Iowa State University, Ames, Iowa 50011, USA*

We use high resolution angle resolved photoemission spectroscopy and density functional theory with measured crystal structure parameters to study the electronic properties of $CaKFe_4As_4$. In contrast to the related $CaFe_2As_2$ compounds, $CaKFe_4As_4$ has a high T_c of 35K at stochiometric composition. This presents a unique opportunity to study the properties of high temperature superconductivity in the iron arsenides in the absence of doping or substitution. The Fermi surface consists of several hole and electron pockets that have range of a diameters. We find that the values of the superconducting gap are nearly isotropic (within the explored portions of the BZ), but are significantly different for each of the FS sheets. Most importantly, we find that the momentum dependence of the gap magnitude plotted across the entire Brillouin zone displays a strong deviation from the simple $\cos(k_x)\cos(k_y)$ functional form of the gap function, proposed by the scenario of Cooper-pairing driven by a short range antiferromagnetic exchange interaction. Instead, the maximum value of the gap is observed on FS sheets that are closest to the ideal nesting condition in contrast to previous observations in other ferropnictides. These results provide strong support for the multiband character of superconductivity in $CaKFe_4As_4$, in which Cooper pairing forms on the electron and the hole bands interacting via a dominant interband repulsive interaction, enhanced by band nesting.

PACS numbers: 74.25.Jb, 74.72.Hs, 79.60.Bm

The superconducting mechanism in iron-based, high temperature superconductors is an important topic in condensed matter physics. One key question is whether the system should be described within a weak coupling BCS-type approach with a key role played by the interband repulsion between electron and hole bands, separated by the large momentum transfer or by a strong coupling approach with dominant short-range antiferromagetic fluctuations described by the local exchange interaction[1–7]. The former scenario seemed consistent with experimental results from a number of iron pnictide superconductors[8], but was later challenged by the discovery of iron chalcogenide-based superconductors[9, 10]. Theoretical progress in this field was inspired by the discovery of new materials in this family [11] from iron chalcogenide[12] to single layer FeSe films[13]. Materials with different crystal or electronic structures are extremely useful and provide new insights for constructing global models of high temperature superconductivity in iron-based materials.

Recently, a new iron-based class of superconductors: $AeAFe_4As_4$ (Ae = Ca, Sr, Eu and A = K, Rb, Cs), were reported (generically referred to as $AeA1144$)[14, 15]. Although the chemical composition of $AeA1144$ is the same as the intensively studied (Ba, K)Fe_2As_2 system, it has a different crystal structure type with Ae and A layers alternatively stacked between Fe_2As_2 layers. The crystallographically inequivalent position of the Ae and A atoms changes the space group from *I4/mmm* to *P4/mmm*. A high transition temperature (T_c = 31 - 36 K) and stochiometric composition makes the $AeA1144$ family an ideal new platform to test existing theories and inspire new ones. Measurements of its electronic structure and the momentum dependence of its superconducting gap are of critical importance.

In this letter, we investigate the band structure and momentum dependence of the superconducting gap of $CaKFe_4As_4$ with high resolution Angle Resolved Photoemission Spectroscopy (ARPES) and DFT using experimentally obtained crystal structure parameters. Unlike most other iron-based superconductors, $CaKFe_4As_4$ has a high T_c of 35 K at stoichiometric composition which allows for the study of iron based high temperature superconductivity in the absence of disorder caused by substitution. The Fermi surface consists of three hole pockets at the Γ point and two electron pockets at the M point. The hole pockets have significantly different diameters, which allows us to measure the superconducting gap for different values of the total momentum $\mathbf{k}$. We find that the superconducting gap is nearly isotropic on each FS sheet, but has a significantly different value for each of the Fermi surface(FS) sheets. Indeed, the largest superconducting gap is found for pairs of hole and electron pockets that have a similar diameter, while other pockets have a smaller value of the superconducting gap. This observation is in stark contrast to the

situation in some other ferropnictides. For example, in LiFeAs, which is another stoichiometric pnictide superconductor with multiple Fermi surface sheets, the largest superconducting gap is found on the smallest hole pocket, located near the zone center.[16, 17] Therefore, our results on $CaKFe_4As_4$ provide a new important ingredient that must be included in the superconducting mechanism of iron-based superconductors.

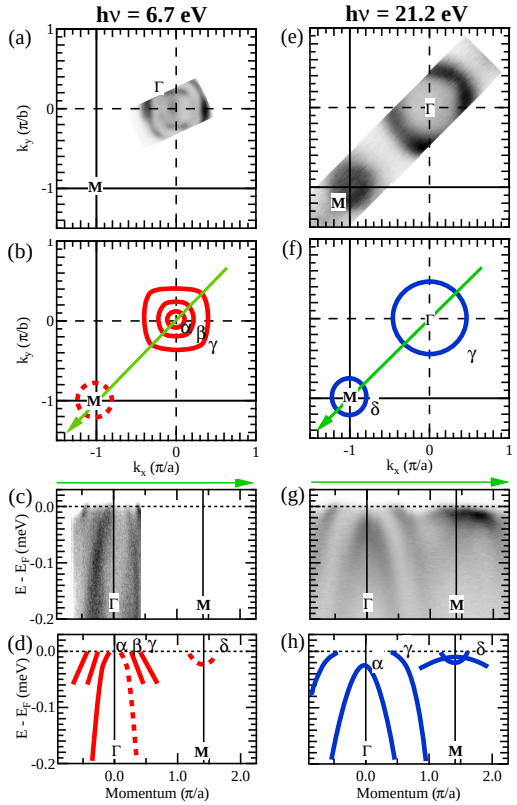

FIG. 1. Measured electronic structure of $CaKFe_4As_4$. (a) Fermi surface intensity acquired using photon energy of 6.7 eV and T=40 K. (b) Sketch of the FS based on data in (a). (c) Measured ARPES intensity along a cut through the Γ point. Cut position is indicated in panel (b). (d) Sketch of the band structure based on data in (c). (e)-(h) Same as (a)-(d), but measured using a photon energy of 21.2 eV. Dashed lines in (b) and (d) mark the expected parts of the bands and FS that are not observed due to matrix elements and limiter access to BZ at low photon energy.

$CaKFe_4As_4$ single crystals were grown using the flux method and extensively characterized by thermodynamic and transport measurements[15, 19]. The experimental structure parameters were obtained from single crystal X-ray diffraction. Technical details are provided in the Supplemental Material. Single phase samples were cleaved *in situ* at a base pressure of lower than 8×10^{-11} Torr. ARPES measurements were performed using a tunable VUV laser spectrometer [20](hν=6.7 eV, ΔE=4 meV) and helium microwave plasma spectrometer ($h\nu$=21.2 eV, ΔE=8 meV). Assuming that $CaKFe_4As_4$

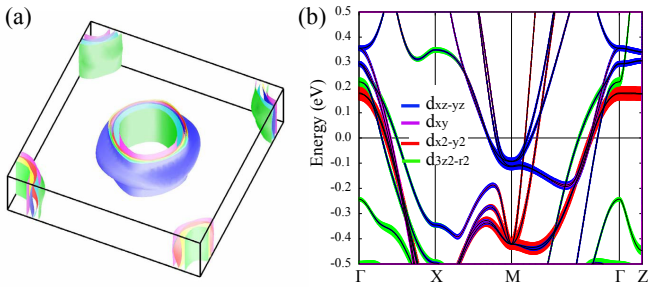

FIG. 2. (a) calculated 3D Fermi surface of $CaKFe_4As_4$ (b-e) band dispersion along the key symmetry directions with respective orbital contributions marked by color coded outlines.

has the same inner potential (∼12 eV) as (Ba,K)Fe_2As_2 then 6.7 eV and 21.2 eV light sources measure the electronic structure around $k_z = \pi$ and $k_z = 0$ respectively [21, 22]. The energy corresponding to the chemical potential was determined from the Fermi edge of a polycrystalline Au reference in electrical contact with the sample. The consistency of the data was confirmed by measuring six different samples.

The measured Fermi surface and band dispersion are shown in Fig. 1. In data collected using a photon energy of 6.7 eV, three hole pockets are observed at the center of the zone (α, β and γ shown in panels (a)-(d)). Whereas the α pocket is fairly round, the shapes of the β and γ pockets are more square-ish. The approximate diameters of these three pockets are ∼0.2 π/a, ∼0.4 π/a and ∼0.8 π/a respectively. The FS and band structure data measured using a photon energy of 21.2 eV are shown in Fig. 1(e)-1(h). At this photon energy, only largest hole pocket around Γ is observed and its diameter is ∼0.45 π/a. The β pockets is not visible, most likely due to unfavorable matrix elements. The band responsible for α hole pocket, is located 30 meV below E_F for this value of k_z (Fig. 1(g)). This is consistent with the 3D character of most inner hole pockets in 122 systems [21, 23]. We note that this change is not due to an increased sensitivity at low photon energies - in such a situation, two copies of the α band would be observed, one below and one above E_F, which is not the case. At the zone corner, a shallow electron FS pocket (δ) is observed (Fig. 2(g)-2(h)).

The Fermi surface and orbitally resolved band dispersion were calculated using Density Functional Theory (DFT) and a Local Density Approximation (LDA)combination with experimental lattice constants and atomic positions (obtained from single crystal X-ray diffraction measurements and shown in Table II of the Supplemental Material.). The resulting FS and band structure are shown in Fig. 2. The calculation predicts six hole pockets – slightly deformed, quasi 2D cylinders centered at the Γ point of the BZ, yet the ARPES data in Fig. 1 shows only three Fermi sheets around Γ. Most likely, the intensity of the β sheet is due to three closely located bands

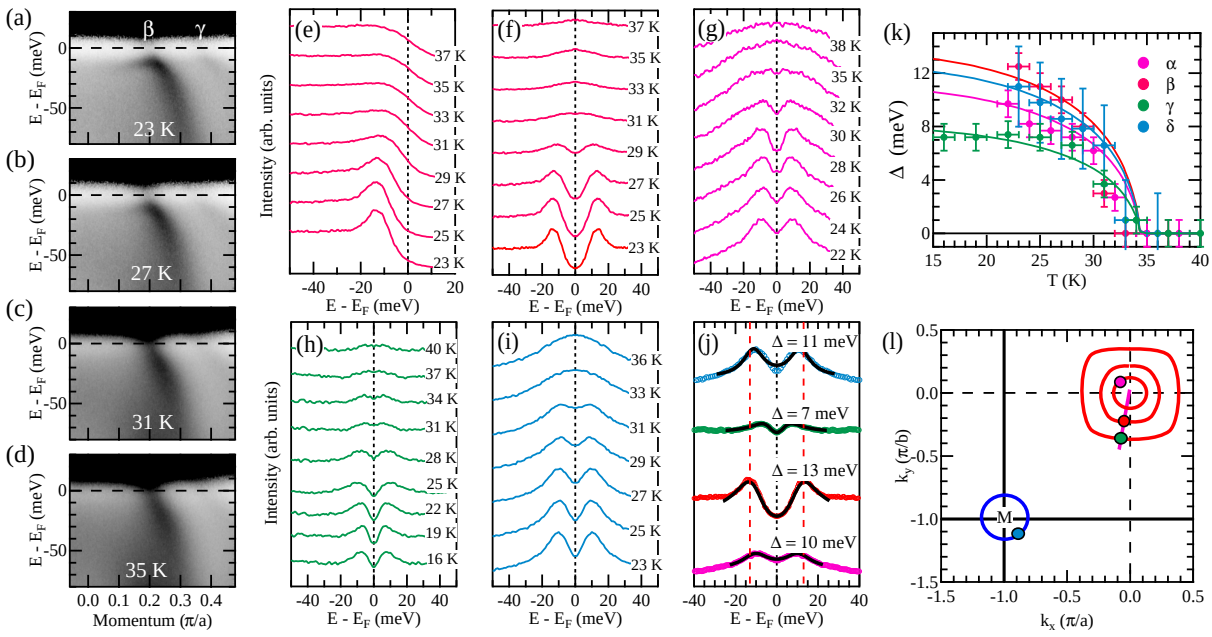

FIG. 3. (a)-(d) Measured electronic structure at four selected temperatures along cut indicated in (l). The data is divided by the Fermi-Dirac function. (e) EDCs at k_F of β FS pocket. (f) The data from panel (e) after symmetrization. (g)-(i) Symmetrized EDCs at k_F of α, γ and δ FS pockets respectively. k_F positions are marked in (l). (j) Symmetrized EDCs at k_F for lowest measured temperature from (f)-(i). Red, vertical dashed lines mark the energy of largest gap (β FS sheet). The black lines are the fits using phenomenological model [18]. (k) Temperature dependence of the superconducting gaps for all four pockets. Solid lines are BCS predictions for Δ_0 of 10.5 meV, 13 meV, 8 meV and 12 meV. (l) Sketch of the FS with indication of the cut position and k_F positions.

that cannot be resolved experimentally. As in many other iron based superconductors, there are several 3d orbitals contributing to the states near the Fermi level. Fig. 2b shows the band dispersion with color coded orbital contributions. Most importantly, in $CaKFe_4As_4$ in addition to the yz/xz and x^2-y^2-orbital contributions to the Fermi surface pockets, there is also a strong admixture of $3z^2-r^2$-states to the α and γ bands, which is somewhat different from the other ferropnictides. In particular, the contribution of the $3z^2-r^2$ orbital to the states near E_F depends sensitively on the Fe ionic positions as the latter are located at the off high-symmetry points in $CaKFe_4As_4$. In fact in this system there are two Fe-As distances in the As-Fe-As layer, which is in contrast to other ferropnictides such as LiFeAs and $CaFe_2As_2$. The calculation predicts four electron pockets centered at the M point. Experimentally, only one pocket can be resolved, due to a significant intrinsic linewidth and the fact that the bottom of these bands is located very close to E_F.

Fig. 3(a)-3(d) shows the measured electronic structure at several typical temperatures along a cut near the Γ point. Due to matrix elements, only the β and γ bands are seen in this cut. Both bands show a clear back bending structure at low temperature (Fig. 3(a)). We plot the Energy Distribution Curves (EDCs) at the k_F for several different temperatures in Fig. 3(e). A sharp quasiparticle peak gradually forms as the temperature is decreased below T_c. We symmetrized the EDCs at k_F as shown in Fig. 3(f)-3(j) prior to performing fitting [24, 25]. A BCS-based, phenomenological model [18] is used to fit the EDCs and extract the gap size. Results are shown in Fig. 3(j)-(k). All gaps follow a BCS-like temperature dependence and close at T_c with $\Delta_{\alpha 0}$ = 10.5 meV, $\Delta_{\beta 0}$ = 13 meV, $\Delta_{\gamma 0}$ = 8 meV and $\Delta_{\delta 0}$=12 meV, which gives rise to the ratio of $2\Delta_0/k_BT_c$ of 7.4, 9.1, 5.6 and 8.4, indicating the superconductivity of $CaKFe_4As_4$ is in the strong coupling regime.

We measured the momentum dependence of the superconducting gap on the β and δ FS sheets, as summarized in Fig. 4, to elucidate the symmetry of the order parameter in $CaFeK_4As_4$. For qualitative analysis, we extract the EDCs at different k_F on the β and δ FS sheets and symmetrize them in Fig. 4 (a) and 4(b). All symmetrized EDCs show a clear dip structure at E_F and the energy positions of the quasiparticle peaks do not show much variation with the FS angle. In Fig. 4(c) we plot the extracted values of the superconducting gap as a function of FS angle. The gap sizes on these two FS pockets have no clear nodes and are roughly isotropic, which directly excludes the possibility of d-wave paring symmetry in $CaFeK_4As_4$ superconductor. In order to check the k_z de-

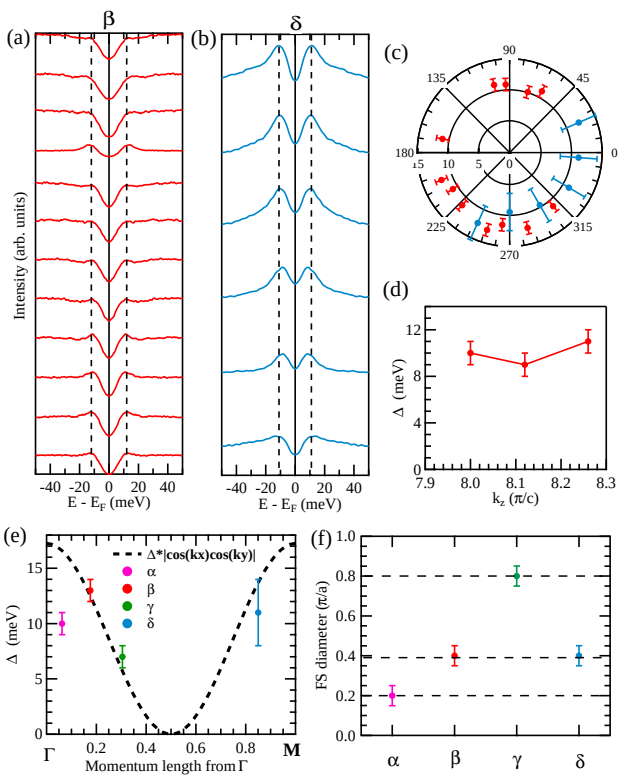

FIG. 4. Momentum dependent superconducting gap. (a)-(b) Symmetrized EDCs at different K_F on the β and δ FS pockets. (c) Extracted superconducting gap from EDCs in (a) and (b). The Γ-X direction is set to 0 degree. (d) k_z dependence of superconducting gap on the β FS pocket. Data were taken with a photon energy of 5.7 eV, 6.2 eV and 6.7 eV. Data in (a)-(d) were taken at 22 K. (e) Plot of the extracted gap on four FS sheets in Fig. 3(j) versus momentum distance from Γ. The black dashed line is a fit with the function $\Delta|cosk_xcosk_y|$, Δ=16 meV. (f) Measured diameters of four Fermi pockets.

pendence of the superconducting gap, we measured the gap size on the β FS with three different photon energies that cover more than $0.2\pi/c$ in momentum space as shown in Fig. 4(d). The gap size does not show much variation within this k_z momentum range either, indicating the quasi-2D nature of $CaFeK_4As_4$.

With the measured amplitude of superconducting gap on all four FS of $CaFeK_4As_4$, we can now check the validity of the previously proposed gap functions. In the strong coupling approach [26, 27], the pairing of electrons occurs because of a short-range interaction. If the antiferromagnetic exchange in iron based superconductors is dominated by next neighbor coupling (J_2) [5], the superconducting gap can be described by a single functional form in the entire Brillouin Zone given by $\Delta(k) = \Delta_0|\cos k_x \cos k_y|$ (or $|\cos k_x + \cos k_y|$ in the 2Fe per unit cell) [26]. Apparently, in this gap function, a FS sheet with a smaller diameter would have a larger superconducting gap around the Brillouin zone center, which is consistent with the measured gap size on the smallest hole pocket in several pnictide superconductors [8, 28, 29]. At the same time, another interpretation of this feature also exists in the purely band description of the $s^{\pm}$-wave superconductivity in which the large size of the superconducting gap on the smallest pocket is attributed to the dominant interband Cooper-pair scattering between electron and hole bands of different sizes. In the absence of direct nesting, the magnitude of the gap is larger on that band, which has a smaller k_F[30, 31]. In Fig. 4(e) we compare the measured gap sizes on different FS with a $\Delta_0|\cos k_x \cos k_y|$ function. The gap size on the α FS is much smaller than the value of the gap, expected from the fit function. (a ∼15 meV gap size is needed to achieve a match.) Therefore the failure of applying the $\Delta_0|\cos k_x \cos k_y|$ function on our measured gap indicates that the superconductivity in $CaFeK_4As_4$ may not be immediately described within the short-range antiferromagnetic fluctuation model. Instead, the measured gaps are consistent with band description of superconductivity. In particular, in contrast to other ferrpnictides some of the bands in $CaFeK_4As_4$ are nested, *i.e.*- the β FS with the largest gap size among three hole FS has the best nesting condition with the δ electron band FS (Fig. 4(f)). It is known theoretically that the nesting between electron and hole bands enhances the repulsive interband interaction between them[1]. Once this interaction becomes larger than the intra-band ones it favors $s^{\pm}$ symmetry of the superconducting gap with gap magnitudes being maximal on the Fermi surfaces that are maximally close to the AF instability, while other gaps on non-nested Fermi surfaces will be smaller.

In the simple mechanism of the $s^{\pm}$ superconducting gap driven by strong inter-band repulsion (which is much bigger than the intra-band interaction due to nesting of the electron and hole bands) the superconducting gaps on each Fermi surface appear to be equal and opposite in sign. Once the intra-band interactions and further Fermi surfaces (not nested) are added, the superconducting gap equations acquires the matrix form and the exact distribution of the gaps on each FS start to depend on various factors such as DOS, orbital content, etc. However, the analysis of these equations in the past [32–35] has shown that the largest gaps always appear on those FSs, which show the largest tendency towards AF instability, which corresponds to nesting of electron and hole bands.

In many of the other iron-based superconductors, xz/yz orbitals contribute mostly to the hole and electron Fermi surfaces near the Γ and M point respectively. Within the $s^{\pm}$ scenario the SC gaps appear to be maximal on these orbitals due strong intra-orbital (inter-band) nesting of the electron and hole pockets. There are, however scenarios (including the s^{++}-wave mechanism[36]) in which nesting does not play an important role and which also predict the largest sc gaps to be on the xz/yz orbitals. One of our most important finding is that in the 1144 compound there are not just xz/yz

orbitals but also z^2 and $x^2 - y^2$, which participate in the intra-orbital inter-band nesting. This provides strong support in favor of the $s^{\pm}$ scenario of superconductivity driven by nesting of the electron and hole bands.

In conclusion, we measured the electronic structure and values of the superconducting gap of a new member of iron arsenic high temperature superconductor - $CaKFe_4As_4$. We find the superconducting gap is nearly isotropic within the explored region of the BZ. The largest gap is observed on the β hole and δ electron sheets, which have very similar diameters, whereas the α and γ sheets have smaller values of the SC gap as they have no electron counterparts of similar diameter. This strongly supports the multiband character of the $s^{\pm}$-wave symmetry of the superconducting gap in which the Cooper-pairing forms on the electron and hole bands with strong interband repulsive interaction, enhanced by the nesting of the electron and hole bands. Raw data for this manuscript is available at http://lib.dr.iastate.edu/ameslab_datasets/.

We would like to thank Rafael Fernandes and Peter Orth for very useful discussions. This work was supported by the U.S. Department of Energy, Office of Science, Basic Energy Sciences, Materials Science and Engineering Division (sample growth, characterization and ARPES measurements). Ames Laboratory is operated for the U.S. Department of Energy by Iowa State University under contract No. DE-AC02-07CH11358. The work of F.L. and I.E. was supported by the joint DFG-ANR Grant No. ER463/8.

[1] A. V. Chubukov, D. V. Efremov, and I. Eremin, Phys. Rev. B **78**, 134512 (2008).
[2] I. Mazin and J. Schmalian, Physica C (Amsterdam) **469**, 614 (2009).
[3] S. Graser, T. A. Maier, P. J. Hirschfeld, and D. J. Scalapino, New Journal of Physics **11**, 025016 (2009).
[4] Q. Si, R. Yu, and E. Abrahams, Nature Reviews Materials **1**, 16017 (2016).
[5] J. Hu, B. Xu, W. Liu, N.-N. Hao, and Y. Wang, Phys. Rev. B **85**, 144403 (2012).
[6] D. S. Inosov, J. T. Park, A. Charnukha, Y. Li, A. V. Boris, B. Keimer, and V. Hinkov, Phys. Rev. B **83**, 214520 (2011).
[7] P. Richard, T. Qian, and H. Ding, Journal of Physics: Condensed Matter **27**, 293203 (2015).
[8] P. Richard, T. Sato, K. Nakayama, T. Takahashi, and H. Ding, Reports on Progress in Physics **74**, 124512 (2011).
[9] D. Mou, L. Zhao, and X. Zhou, Frontiers of Physics **6**, 410 (2011).
[10] D. Liu, W. Zhang, D. Mou, J. He, Y.-B. Ou, Q.-Y. Wang, Z. Li, L. Wang, L. Zhao, S. He, Y. Peng, X. Liu, C. Chen, L. Yu, G. Liu, X. Dong, J. Zhang, C. Chen, Z. Xu, J. Hu, X. Chen, X. Ma, Q. Xue, and X. Zhou, Nat Commun **3**, 931 (2012).
[11] Y. Kamihara, T. Watanabe, M. Hirano, and H. Hosono, J. Am. Chem. Soc. **130**, 3296 (2008).
[12] J. Guo, S. Jin, G. Wang, S. Wang, K. Zhu, T. Zhou, M. He, and X. Chen, Phys. Rev. B **82**, 180520 (2010).
[13] Q.-Y. Wang, Z. Li, W.-H. Zhang, Z.-C. Zhang, J.-S. Zhang, W. Li, H. Ding, Y.-B. Ou, P. Deng, K. Chang, J. Wen, C.-L. Song, K. He, J.-F. Jia, S.-H. Ji, Y.-Y. Wang, L.-L. Wang, X. Chen, X.-C. Ma, and Q.-K. Xue, Chinese Physics Letters **29**, 037402 (2012).
[14] A. Iyo, K. Kawashima, T. Kinjo, T. Nishio, S. Ishida, H. Fujihisa, Y. Gotoh, K. Kihou, H. Eisaki, and Y. Yoshida, J. Am. Chem. Soc. **138**, 3410 (2016).
[15] W. R. Meier, T. Kong, U. S. Kaluarachchi, V. Taufour, N. H. Jo, G. Drachuck, A. E. Böhmer, S. M. Saunders, A. Sapkota, A. Kreyssig, M. A. Tanatar, R. Prozorov, A. I. Goldman, F. F. Balakirev, A. Gurevich, S. L. Bud'ko, and P. C. Canfield, Phys. Rev. B **94**, 064501 (2016).
[16] S. V. Borisenko, V. B. Zabolotnyy, A. A. Kordyuk, D. V. Evtushinsky, T. K. Kim, I. V. Morozov, R. Follath, and B. Büchner, Symmetry **4**, 251 (2012).
[17] K. Umezawa, Y. Li, H. Miao, K. Nakayama, Z.-H. Liu, P. Richard, T. Sato, J. B. He, D.-M. Wang, G. F. Chen, H. Ding, T. Takahashi, and S.-C. Wang, Phys. Rev. Lett. **108**, 037002 (2012).
[18] H. Matsui, T. Sato, T. Takahashi, S.-C. Wang, H.-B. Yang, H. Ding, T. Fujii, T. Watanabe, and A. Matsuda, Phys. Rev. Lett. **90**, 217002 (2003).
[19] T. Kong, W. R. Balakirev, Fedor F.and Meier, S. L. Bud'ko, A. Gurevich, and P. C. Canfield, (2016), arXiv:1606.02241.
[20] R. Jiang, D. Mou, Y. Wu, L. Huang, C. D. McMillen, J. Kolis, H. G. Giesber, J. J. Egan, and A. Kaminski, Review of Scientific Instruments **85**, 033902 (2014).
[21] C. Liu, T. Kondo, N. Ni, A. D. Palczewski, A. Bostwick, G. D. Samolyuk, R. Khasanov, M. Shi, E. Rotenberg, S. L. Bud'ko, P. C. Canfield, and A. Kaminski, Phys. Rev. Lett. **102**, 167004 (2009).
[22] T. Shimojima, F. Sakaguchi, K. Ishizaka, Y. Ishida, T. Kiss, M. Okawa, T. Togashi, C.-T. Chen, S. Watanabe, M. Arita, K. Shimada, H. Namatame, M. Taniguchi, K. Ohgushi, S. Kasahara, T. Terashima, T. Shibauchi, Y. Matsuda, A. Chainani, and S. Shin, Science **332**, 564 (2011).
[23] R. S. Dhaka, C. Liu, R. M. Fernandes, R. Jiang, C. P. Strehlow, T. Kondo, A. Thaler, J. Schmalian, S. L. Bud'ko, P. C. Canfield, and A. Kaminski, Phys. Rev. Lett. **107**, 267002 (2011).
[24] M. R. Norman, H. Ding, M. Randeria, J. C. Campuzano, T. Yokoya, T. Takeuchi, T. Takahashi, T. Mochiku, K. Kadowaki, P. Guptasarma, and D. G. Hinks, Nature **392**, 157 (1998).
[25] T. Kondo, R. Khasanov, T. Takeuchi, J. Schmalian, and A. Kaminski, Nature **457**, 296 (2009).
[26] J. Hu and H. Ding, Scientific Reports **2**, 381 (2012).
[27] Z. P. Yin, K. Haule, and G. Kotliar, Nat Phys **10**, 845 (2014).
[28] H. Ding, P. Richard, K. Nakayama, K. Sugawara, T. Arakane, Y. Sekiba, A. Takayama, S. Souma, T. Sato, T. Takahashi, Z. Wang, X. Dai, Z. Fang, G. F. Chen, J. L. Luo, and N. L. Wang, Europhysics Letters **83**, 47001 (2008).
[29] L. Zhao, H.-Y. Liu, W.-T. Zhang, J.-Q. Meng, X.-W. Jia, G.-D. Liu, X.-L. Dong, G.-F. Chen, J.-L. Luo, N.-

L. Wang, W. Lu, G.-L. Wang, Y. Zhou, Y. Zhu, X.-Y. Wang, Z.-Y. Xu, C.-T. Chen, and X.-J. Zhou, Chinese Physics Letters **25**, 4402 (2008).
[30] X. Chen, S. Maiti, A. Linscheid, and P. J. Hirschfeld, Phys. Rev. B **92**, 224514 (2015).
[31] A. V. Chubukov, I. Eremin, and D. V. Efremov, Phys. Rev. B **93**, 174516 (2016).
[32] P. J. Hirschfeld, M. M. Korshunov, and M. I. I., Rep. Prog. Phys. **74**, 224505 (2011).
[33] S. Maiti, M. M. Korshunov, T. A. Maier, P. J. Hirschfeld, and A. V. Chubukov, Phys. Rev. B **84**, 224505 (2011).
[34] A. V. Chubukov, Annu. Rev. Condens. Matter Phys. **3**, 57 (2012).
[35] F. Ahn, I. Eremin, J. Knolle, V. B. Zabolotnyy, S. V. Borisenko, B. Büchner, and A. V. Chubukov, Phys. Rev. B **89**, 144513 (2014).
[36] H. Kontani and S. Onari, Phys. Rev. Lett. **104**, 157001 (2010).
[37] See Supplemental Material [url], which includes Refs. [38–45].
[38] S. p. Bruker, Version 8.30. Bruker AXS Inc., M., Wisconsin, USA. (2013).
[39] G. M. Sheldrick, SADABS, University of Grottingen, Germany (1996).
[40] Bruker, SMART for Windows NT/2000. Version 6.148. Bruker AXS Inc., M., Wisconsin, USA. (2002).
[41] V. Petricek, M. Dusek, L. Palatinus, and Jana2006, The crystallographic computing system Institute of Physics, Praha, Czech Republic (2006).
[42] L. Palatinus and G. Chapuis, Superflip - a computer program for the solution of crystal structures by charge flipping in arbitrary dimensions (2007).
[43] B. Saparov, C. Cantoni, M. Pan, T. C. Hogan, W. R. Li, S. D. Wilson, K. Fritsch, M. Tachibana, B. D. Gaulin, and A. S. Sefat, Scientific Reports **4**, 4120 (2014).
[44] K. Sasmal, B. Lv, B. Lorenz, A. M. Guloy, F. Chen, Y.-Y. Xue, and C. W. Chu, Physical Review Letters **101**, 107007 (2008).
[45] A. Iyo, K. Kawashima, T. Kinjo, T. Nishio, S. Ishida, H. Fujihisa, Y. Gotoh, K. Kihou, H. Eisaki, and Y. Yoshida, J. Am. Chem. Soc. **138**, 3410.